Impact of Atmosphere and Land Surface Initial Conditions on Seasonal Forecasts of Global Surface Temperature

STEFANO MATERIA, ANDREA BORRELLI, ALESSIO BELLUCCI, AND ANDREA ALESSANDRI*

Centro Euro-Mediterraneo sui Cambiamenti Climatici, Bologna, Italy

PIERLUIGI DI PIETRO

Istituto Nazionale di Geofisica e Vulcanologia, Bologna, Italy

PANAGIOTIS ATHANASIADIS

Centro Euro-Mediterraneo sui Cambiamenti Climatici, Bologna, Italy

ANTONIO NAVARRA AND SILVIO GUALDI

Centro Euro-Mediterraneo sui Cambiamenti Climatici, and Istituto Nazionale di Geofisica e Vulcanologia, Bologna, Italy

(Manuscript received 5 March 2014, in final form 13 September 2014)

ABSTRACT

The impact of land surface and atmosphere initialization on the forecast skill of a seasonal prediction system is investigated, and an effort to disentangle the role played by the individual components to the global predictability is done, via a hierarchy of seasonal forecast experiments performed under different initialization strategies. A realistic atmospheric initial state allows an improved equilibrium between the ocean and overlying atmosphere, increasing the model predictive skill in the ocean. In fact, in regions characterized by strong air–sea coupling, the atmosphere initial condition affects forecast skill for several months. In particular, the ENSO region, eastern tropical Atlantic, and North Pacific benefit significantly from the atmosphere initialization. On the mainland, the effect of atmospheric initial conditions is detected in the early phase of the forecast, while the quality of land surface initialization affects forecast skill in the following seasons. Winter forecasts in the high-latitude plains benefit from the snow initialization, while the impact of soil moisture initial state is particularly effective in the Mediterranean region and central Asia.

However, the initialization strategy based on the full value technique may not be the best choice for land surface, since soil moisture is a strongly model-dependent variable: in fact, initialization through land surface reanalysis does not systematically guarantee a skill improvement. Nonetheless, using a different initialization strategy for land, as opposed to atmosphere and ocean, may generate inconsistencies. Overall, the introduction of a realistic initialization for land and atmosphere substantially increases skill and accuracy. However, further developments in the procedure for land surface initialization are required for more accurate seasonal forecasts.

1. Introduction

Seasonal scale has recently become a crucial time frame for climate forecast, owing to its socioeconomic relevance. In the last decade, important advances have been achieved, thanks to the development of fully coupled general circulation models (CGCMs) initialized for seasonal prediction (Kug et al. 2008; Kim et al. 2012). Dynamical predictions are based on the assumption that large-scale and long-lasting anomalies will convey predictive skill to seasonal forecast. In particular, the ocean provides ''hidden'' memory to the climate system (Hoskins and Schopf 2008), enabling fully coupled models to produce skillful predictions up to one year ahead or more (Blender and Fraedrich 2003).

* Current affiliation: Agenzia Nazionale per le Nuove Tecnologie, l'Energia e lo Sviluppo Economico Sostenibile, Rome, Italy.

Corresponding author address: Stefano Materia, Centro Euro-Mediterraneo per i Cambiamenti Climatici, Viale Aldo Moro, 44, Bologna, 40141, Italy.
E-mail: stefano.materia@cmcc.it

DOI: 10.1175/JCLI-D-14-00163.1

Currently, most ocean initialization strategies are based on analyses that assimilate observed temperature, salinity, and sea level data via multivariate schemes, imposing physical and dynamical constraints among different variables (Balmaseda et al. 2009). Accuracy in the knowledge of the ocean initial state led to a fundamental progress in the understanding of coupled ocean–atmosphere interaction mechanisms (McPhaden et al. 1998), and the use of assimilated subsurface temperature and salinity profiles to initialize the ocean contributed to increase seasonal forecast skill (Alves et al. 2004; Vidard et al. 2007; Alessandri et al. 2010). Although anomalous conditions in each ocean basin can have significant effects on climate (Iwi et al. 2006), the largest source of seasonal forecast skill is El Niño–Southern Oscillation (ENSO; Smith et al. 2012), which exerts a global influence on seasonal climate through teleconnections (Trenberth and Caron 2000).

In the last 15 years, the role played by land surface processes has received growing attention in the seasonal prediction community: initial state of snow cover, soil wetness, and other land surface variables have a major influence on seasonal mean circulation (Fennessy and Shukla 1999). There is reasonable confidence that prior knowledge of land surface state yields significant skill in forecasting seasonal soil moisture and surface temperature (Koster and Suarez 2003; Douville 2003; Jeong et al. 2008). However, whether soil moisture can drive some predictability of precipitation anomalies at such a time scale is still an open question (Paolino et al. 2012). Koster and Suarez (2004) indicate that a global model forecast of precipitation may be greatly improved with a global initialization of soil moisture. Other studies have suggested that in limited regions of the world, referred to as "hot spots," knowledge of antecedent anomalies of the land surface state can result in an improved forecast of seasonal precipitation anomalies (Koster et al. 2004, 2010; Alessandri and Navarra 2008).

In addition to the role played by ocean and land surface memory, the atmosphere may enhance large-scale predictability interacting with the slowly evolving oceanic component (e.g., Navarra 2002; Shukla and Kinter 2006). Also, changes in planetary wave structure, determined by atmospheric teleconnectivity, can propagate climate variability on monthly time scales between distant regions of the globe (e.g., Palmer et al. 2008), and models' predictive skill may benefit from this information. However, Dirmeyer (2003) estimates that the contribution to forecast skill from the atmospheric state in a coupled land–atmosphere model with specified sea surface temperatures (SSTs) decays in less than a month, with longer skill due only to land initial condition.

Ultimately, the impact of initialization is strongly dependent on the quality of the coupled model (Balmaseda et al. 2009) and its capacity to reproduce observed processes. In a review on operational forecasts for the 1997/98 El Niño, Trenberth (1998) concludes that the systems that performed best were based on advanced coupled dynamical models of the ocean and atmosphere.

In this study, we primarily intend to examine the quality of seasonal forecasts obtained by the introduction of land surface and atmosphere initial conditions in the most recent version of the Centro Euro-Mediterraneo sui Cambiamenti Climatici (CMCC) Seasonal Prediction System, version 2 (CMCC-SPSv2; Borrelli et al. 2012). In addition, we make an attempt to determine the relative contribution of land surface and atmosphere to predictability at a seasonal time scale by separating the impact of the two components.

The paper is organized as follows. Section 2 describes the CMCC-SPS physical core, the experimental design, and the methods used to assess of the model skill and accuracy. Section 3 documents the improvements in the CMCC-SPS predictive skill introduced by the initialization of land surface and atmosphere, compared with the previous version where only the ocean state was initialized. In section 4 we quantify the relative contribution of land surface and atmosphere initialization on the overall predictive skill of the system. Finally, concluding remarks are provided in section 5.

2. The CMCC Seasonal Prediction System

a. *Main components of the global model*

The main components of the CMCC coupled global circulation model are summarized in Fig. 1. The atmospheric component consists of the ECHAM5.3 model (Roeckner et al. 2003, 2006) at spectral T63 horizontal resolution, with 19 vertical levels. The atmosphere is directly coupled to the land surface scheme Surface Interactive Land Vegetation (SILVA; Alessandri et al. 2012) at the same horizontal grid.

The ocean model is Océan Parallélisé version 8.2 (OPA8.2; Madec et al. 1998), run on a standard ORCA2 grid (Madec and Imbard 1996) of about 2° and 31 vertical levels. The Arctic sea ice is driven by SSTs, through a function that determines the water freezing point.

The atmosphere and the ocean models communicate with each other through the Ocean Atmosphere Sea Ice Soil version 3 (OASIS3) coupler (Valcke et al. 2000), and no flux corrections are applied. Specific aspects of the ocean–atmosphere coupling are discussed in Fogli et al. (2009), and more details about the CMCC-SPS physical core can be found in Borrelli et al. (2012).

b. *Experimental design*

A set of retrospective forecasts (hindcasts) was performed for the 1989–2005 period, using three different

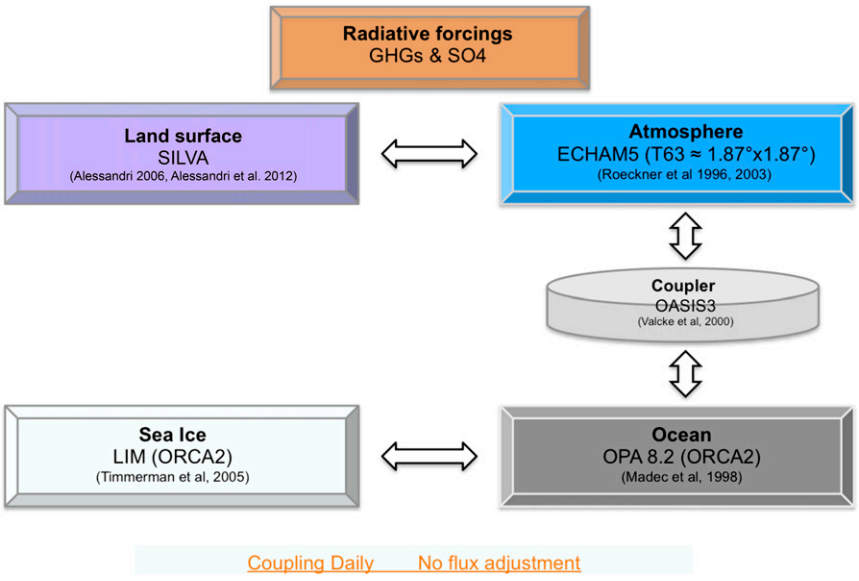

FIG. 1. Main components of the CMCC-SPS coupled model.

configurations of the CMCC-SPS, based on distinct initialization strategies (Table 1). In CMCC-SPS version 1 (CMCC-SPSv1, hereinafter SPS1; Alessandri et al. 2010, 2011) only the ocean was initialized with a realistic state estimate based on the CMCC–Istituto Nazionale di Geofisica e Vulcanologia (INGV) Global Data Assimilation (CIGODAS) reanalysis (Bellucci et al. 2007; Masina et al. 2011). CIGODAS is based on an optimal interpolator scheme, assimilating in situ temperature and salinity profiles, and forced with fluxes from the European Centre for Medium-Range Weather Forecasts (ECMWF) operational analysis. Initial conditions for land and atmosphere are obtained through an Atmospheric Model Intercomparison Project (AMIP)-type simulation, performed by forcing the atmospheric model with observed SST from the Met Office Hadley Centre Sea Ice and Sea Surface Temperature global dataset, version 1.1 (HadISST1.1; Rayner et al. 2006). Sea ice cover is empirically diagnosed at the onset of the forecast from the SST analysis, while sea ice thickness and snow depth over ice are set to a 1989–2008 climatology derived from an historical simulation of the 1960–2008 climate, carried out with the same dynamical model of the SPS1 system.

To evaluate the impact of atmosphere initialization, an additional set of seasonal forecast experiments was performed, where, in addition to the ocean (initialized as in the control SPS1 experiment), also the atmosphere is provided with observed initial conditions. Here, the state of the atmosphere is given by the ECMWF Interim Re-Analysis (ERA-Interim, hereinafter ERAI; Berrisford et al. 2009). As for SPS1, sea ice and land surface state variables are initialized with a model climatology and a forced AMIP-type simulation, respectively. The corresponding system is labeled as CMCC-SPSv1.5 (hereinafter SPS1.5).

Finally, a third set of seasonal prediction experiments, based on the CMCC-SPSv2 (Borrelli et al. 2012, hereinafter SPS2), was produced, where a realistic initialization for land surface conditions is provided in addition to ocean and atmosphere. Consistently with the above atmosphere, snow depth, soil moisture, and soil temperature are initialized using the ERAI.

Snow depth and surface temperature at the interface with the atmosphere are started with the corresponding ERAI fields. As for soil moisture, we use the wetness of the four soil layers included in Hydrology Tiled ECMWF Scheme for Surface Exchanges over Land (HTESSEL, i.e., the land surface model used in the ECMWF reanalysis system; Balsamo et al. 2009) to estimate the water content into the two soil reservoirs implemented in SILVA. The water content, relative to saturation condition, in the upper (lower) soil layers of SILVA is computed as the weighted average of the soil wetness in layers 1 and 2 (3 and 4) of HTESSEL. To match the soil moisture characteristic of the coupled model, ERAI values were weighted over field capacity

TABLE 1. The set of experiments with indication of the initialized component.

Initialization	SPS1	SPS1.5	SPS2
Ocean	CIGODAS	CIGODAS	CIGODAS
Atmosphere	AMIP	ERAI	ERAI
Land surface	AMIP	AMIP	ERAI

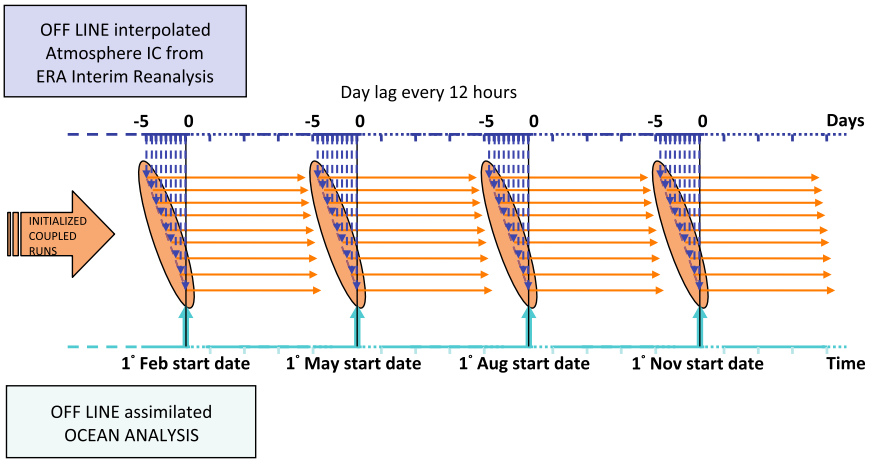

FIG. 2. SPS2 experimental setup. Readapted from Alessandri et al. (2010).

and wilting point, in order to obtain a soil moisture index comparable to SILVA and avoid inconsistencies.

In each of the abovementioned systems, the model is initialized every year at four different start dates (on the first of February, May, August, and November; Fig. 2) and then integrated for six months. To account for the uncertainty characterizing the initial state of the system, an ensemble of nine perturbed atmospheric initial conditions was prepared for each start date. Specifically, the atmospheric condition is perturbed, by imposing the state observed at 12 h, 24 h, and so on up to 108 h before the start date (see Fig. 2). In this way, the dynamical model evolves from nine different initial states, producing an ensemble of forecasts. In the following analysis we only focus on May and November start dates, assessing the predictive capability of the CMCC-SPS for summer and winter seasons, respectively.

c. Verification: Methodology and data

Two statistical metrics are used to quantitatively assess the performance of CMCC-SPS: the anomaly correlation coefficient (ACC) and the root-mean-square error (RMSE). ACC [Eq. (1)] is used to evaluate the forecast skill, namely the capability of the model to make a prediction, and is defined as follows:

$$\mathrm{ACC}(\tau) = \frac{\sum_{y=1}^{Y} x'_y(\tau) o'_y(\tau)}{\sqrt{\sum_{y=1}^{Y} x'^2_y(\tau) o'^2_y(\tau)}}, \qquad (1)$$

where τ represents the lead season (see section 3) to which ACC refers, x' and o' respectively indicate predicted and observed anomalies, computed by subtracting the respective monthly climatologies, and y is the forecast year (total number of years $Y = 17$).

RMSE is a measure of accuracy. It is defined as the distance between the forecast and the observational dataset:

$$\mathrm{RMSE}(\tau) = \sqrt{\frac{1}{Y}\sum_{y=1}^{Y} [x'_y(\tau) - o'_y(\tau)]^2}. \qquad (2)$$

The RMSE, in contrast to ACC, is negatively oriented (i.e., an increasing numerical value indicates a worsening of the prediction).

The predictive skill of the system is verified versus the ERAI, which hereafter will be simply referred to as observations. Anomalies in both forecasts and observations are defined as deviations from the 1989–2005 climatology.

3. The impact of land–atmosphere initialization

a. Global view

In this section, the performance of SPS2 in terms of predictive skill and accuracy is evaluated, and compared with the skill of the control system, SPS1. Each analysis is here computed for the ensemble mean forecast.

In Fig. 3, we show ACC maps for SPS2 surface temperature. The plots refer to lead season 1, that is the trimonthly mean starting one month after the start date (i.e., lead season 1 for February represents the March–May average). At first glance, the skill in the tropics looks higher than at mid and high latitudes, and correlations over the ocean are typically larger than over land. The central equatorial Pacific is the region where SPS2 features the largest skill. Significantly high correlations are also found over the northwestern Pacific and North Atlantic. Over land, the strongest correlations in all the

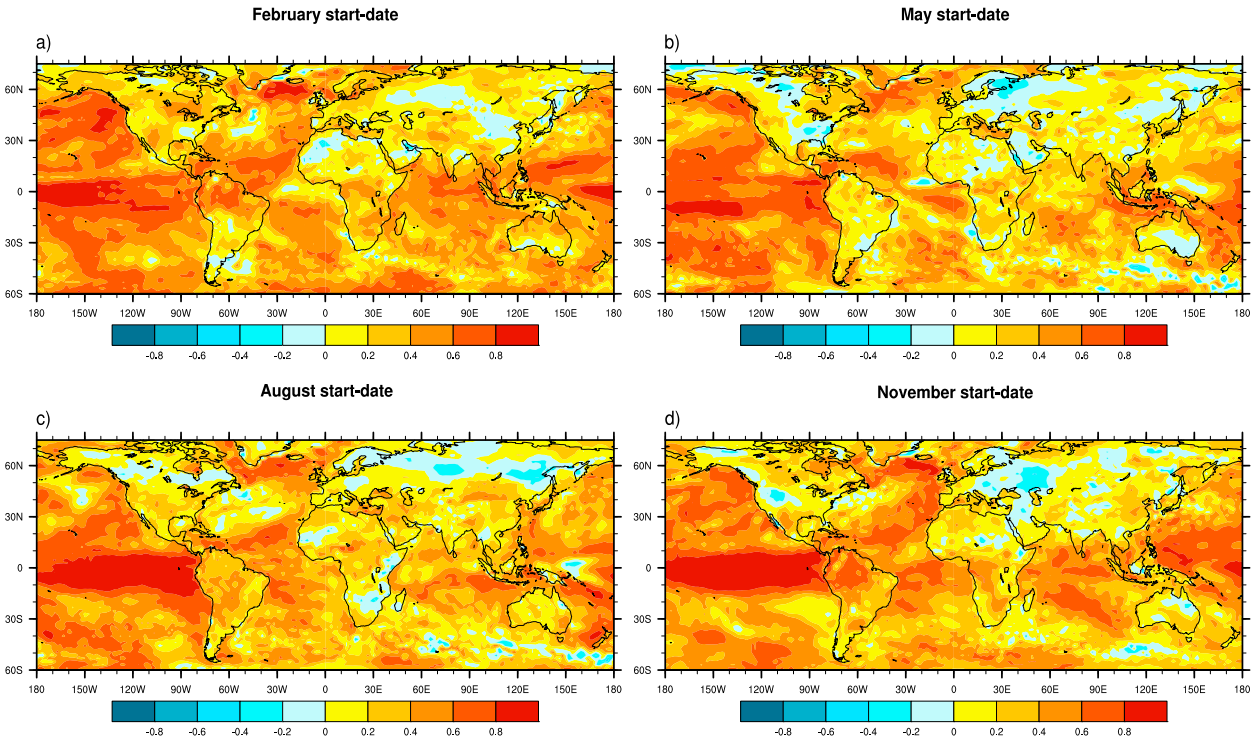

FIG. 3. ACC of surface temperature in CMCC-SPSv2 vs ERAI. All plots refer to the forecast for lead season 1.

start dates are found in the Amazon basin. On the other hand, there are vast continental areas featuring negative ACC values (corresponding to no skill).

Figures 4 and 5 display differences between ACC patterns for surface temperatures in SPS1 and SPS2 for May and November start dates. Red (blue) color indicates an increase (decrease) of ACC in SPS2 with respect to SPS1. Each difference is based on the ensemble mean of the nine members, which represents the deterministic realization of the forecast probability distribution. In the maps, only values significant at the 95% confidence level are plotted.

Compared to SPS1, SPS2 provides a remarkable improvement of the forecast skill at lead season 0 (i.e., the trimonthly mean starting at the same time as the start date; Figs. 4a, 5a). Through the realistic initialization of the atmospheric GCM component (using ERAI), a coupled equilibrium state between the ocean and overlying atmosphere is reached more quickly. This may contribute to improve the transient response to initialization, mitigating the spurious coupling shock which often arises as a consequence of the full-value initialization strategy (Troccoli et al. 2008), ultimately enhancing the skill in the early phase of the forecast.

In many ocean regions, mainly in the November start date, improvements are not restricted to lead season 0, but tend to persist throughout the forecast (Figs. 5c,d). The Pacific Ocean, with particular regard to the central northern and southeastern tropical and subtropical sectors, undergoes large improvements. In the autumnal forecast, also large part of the Atlantic sector and the Southern Ocean benefit from the upgraded initialization. In the May start date (Figs. 4c,d), durable improvements are remarkable in the upwelling regions off the coasts of North and South America and in the northern tropical Atlantic. On the other hand, SPS2 ACC is lower in the western equatorial Pacific (August start date; not shown), central Pacific (Figs. 4c,d), and a few sections of the Indian Ocean (Fig. 4b).

Most of the continental areas, mainly in North America, Asia, and generally in the Southern Hemisphere, appear to considerably benefit from the upgraded initial state in the initial lead season. The latter is strongly influenced by the first forecast month (lead month 0) and a decrease in the spatial extent of improvements is evident starting from lead season 1. Only in a few regions, in fact, do variations driven by the different initialization strategy seem to last throughout the forecast. Long-lasting improvements are particularly evident in Eurasia, whereas in northern Africa and Australia the forecast is often deteriorated by the upgraded initialization.

Figures 6 and 7 show RMSE differences between surface temperatures in SPS1 and SPS2. In this case, the color code is reversed with respect to ACC maps, in order to maintain the red (blue) color as an indication

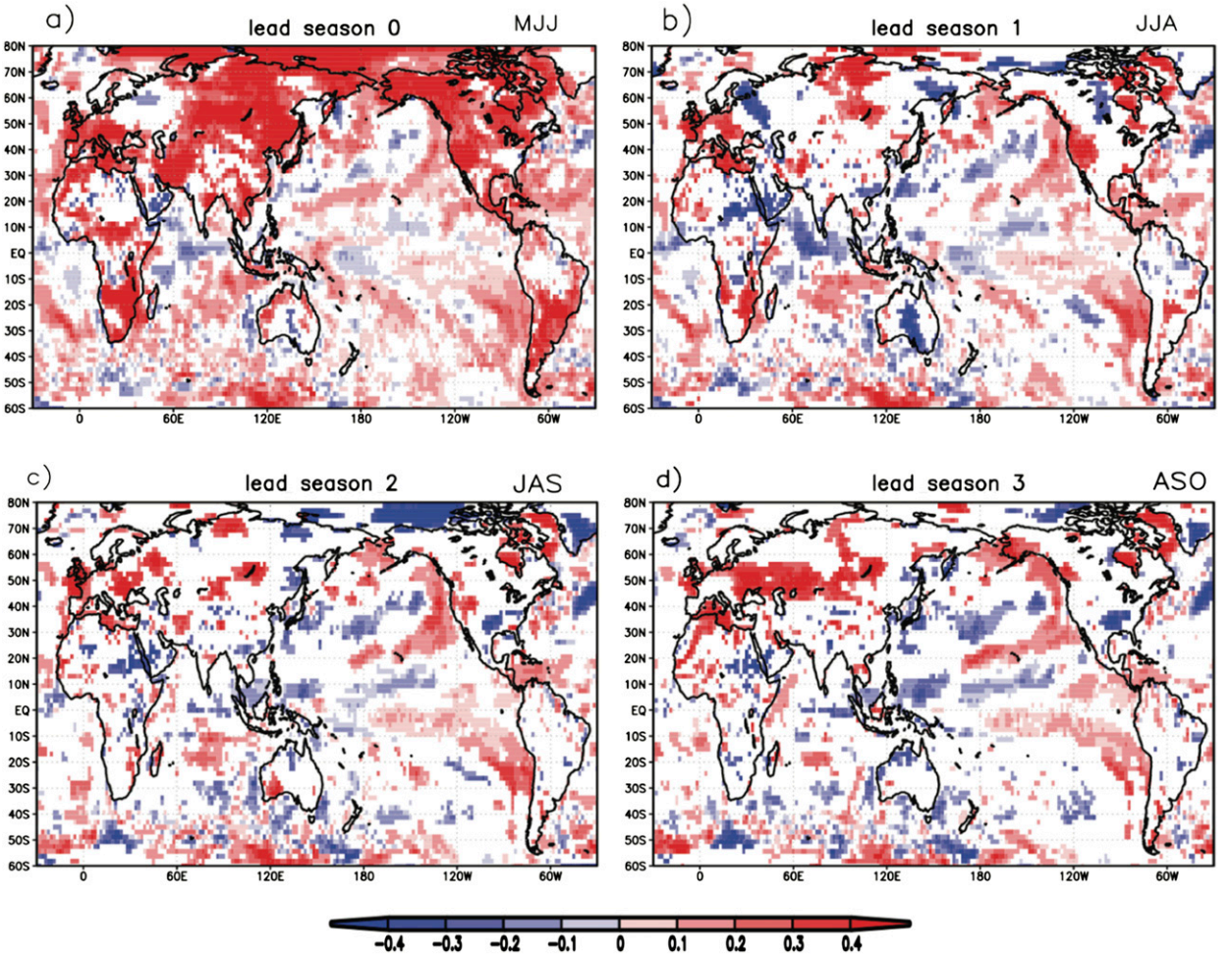

FIG. 4. ACC difference between SPS2 and SPS1 for the start date of May, lead seasons 0–3. Shaded areas indicate differences significant at the 95% confidence level.

of improvement (deterioration) imparted by land–atmosphere original state. The forecast accuracy is again largely improved in the initial lead seasons because of the contribution of the first lead month (Figs. 6a, 7a). Differences in the global picture mirror the differences shown in terms of ACC.

From lead season 1 onward, with the exception of the regions mentioned, the skill and accuracy increase/decrease are less consistent, with frequent variations depending on the area and the start date (Figs. 6c,d and 7c,d). An integral description of ACC and RMSE changes, determined by the different initialization strategies implemented in SPS1 and SPS2, separately for land, oceans, and the global domain is shown in Fig. 8.

At the global scale, SPS2 generally exhibits more skill and accuracy compared to SPS1 for the entire 6-month period, although improvements tend to decline after one or two months and become small by the end of the forecast. Skill amelioration is particularly pronounced for May start date, whereas the forecast starting in August does not benefit substantially from the observational initial condition.

On land, the large improvement in SPS2 skill and accuracy at lead month 0 becomes less remarkable in the following seasons. Here, the strongest impact of land–atmosphere initialization is evident for the November start date. Especially in February and May, performance of SPS2 quickly declines after initialization, and becomes very similar to that of SPS1. Yet, predictive skill starts increasing again from the third month after the initialization. In the ocean, differences between SPS1 and SPS2 are more regular throughout the entire forecast time, except for the start date of February, which receives a remarkable push from the realistic land and atmosphere initial state.

b. *ENSO region*

Since the main driver of the global interannual SST variance is the variability in the equatorial Pacific

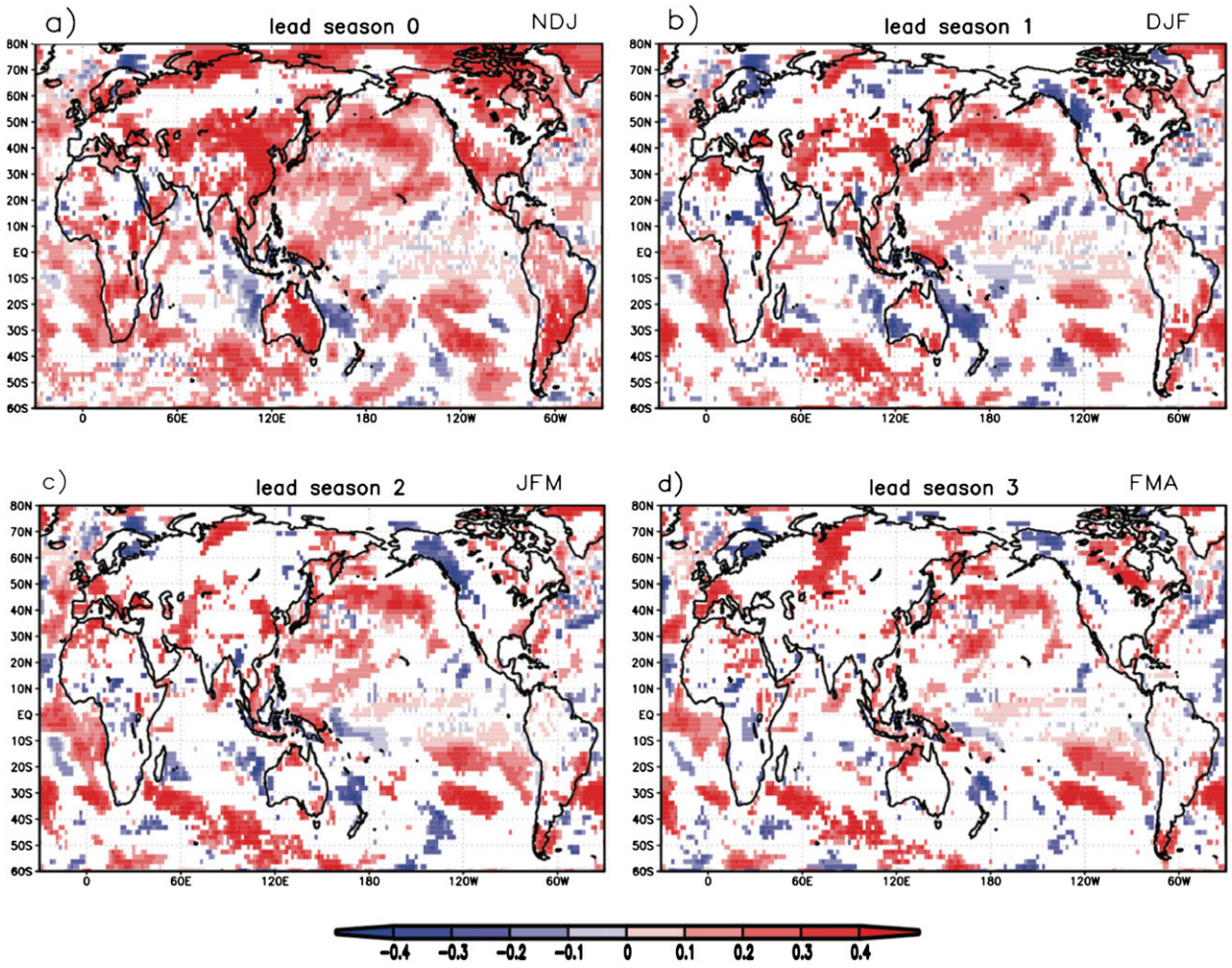

FIG. 5. As in Fig. 4, but for the start date of November.

associated with ENSO, the seasonal prediction skill in this region is crucial for reliable forecasts. In both SPS models, the central and eastern equatorial Pacific are characterized by ACC values close to 1 up to the last lead season, especially in the initializations of August (not shown) and November (Fig. 3).

Skill and accuracy associated with the Niño-3.4 SST index for SPS2, is shown in Fig. 9 (bottom and top panels, respectively). The introduction of the atmospheric initialization improves notably the SPS2 predictive performance, especially in the May start date (Figs. 9a,c). Within the forecast set, the latter is the start date with the lowest forecast skill and the largest RMSE, in reason of the seasonal dependency of the equatorial Pacific SST predictability: the so-called spring barrier has long been documented in ENSO forecast as a drop of skill persistence across the boreal spring (Chen et al. 2004). The CMCC-SPS is affected by the same limitation. This is also confirmed by the curve of persistent forecast that quickly drops to insignificant correlation values, indicating a disconnection to the initial state. Instead, the ACC curve of persistence remains above 0.6 up to the sixth month after the initializations of November (Fig. 5d), demonstrating higher SST predictability for this forecast.

As mentioned before, the introduction of realistic land–atmosphere initial conditions determines a remarkable upgrade of the ENSO forecast for June–August (JJA), statistically significant at lead season 1 (Table 2). Improved predictive skill and accuracy of this region could be ascribed to the intraseasonal stochastic component introduced by the atmospheric initial state, as in Shi et al. (2011), who found an important impact on predictability of the 1997 El Niño early warming. In addition, the lack of correct initialization could lead to the amplification of initial condition errors, especially in a system characterized by such a coupling between ocean and atmosphere (Hudson et al. 2011).

Differences in the Niño-3.4 index forecast between SPS1 and SPS2 are small, but still noticeable, as shown in Fig. 10. We show only lead season 1 for the start date of

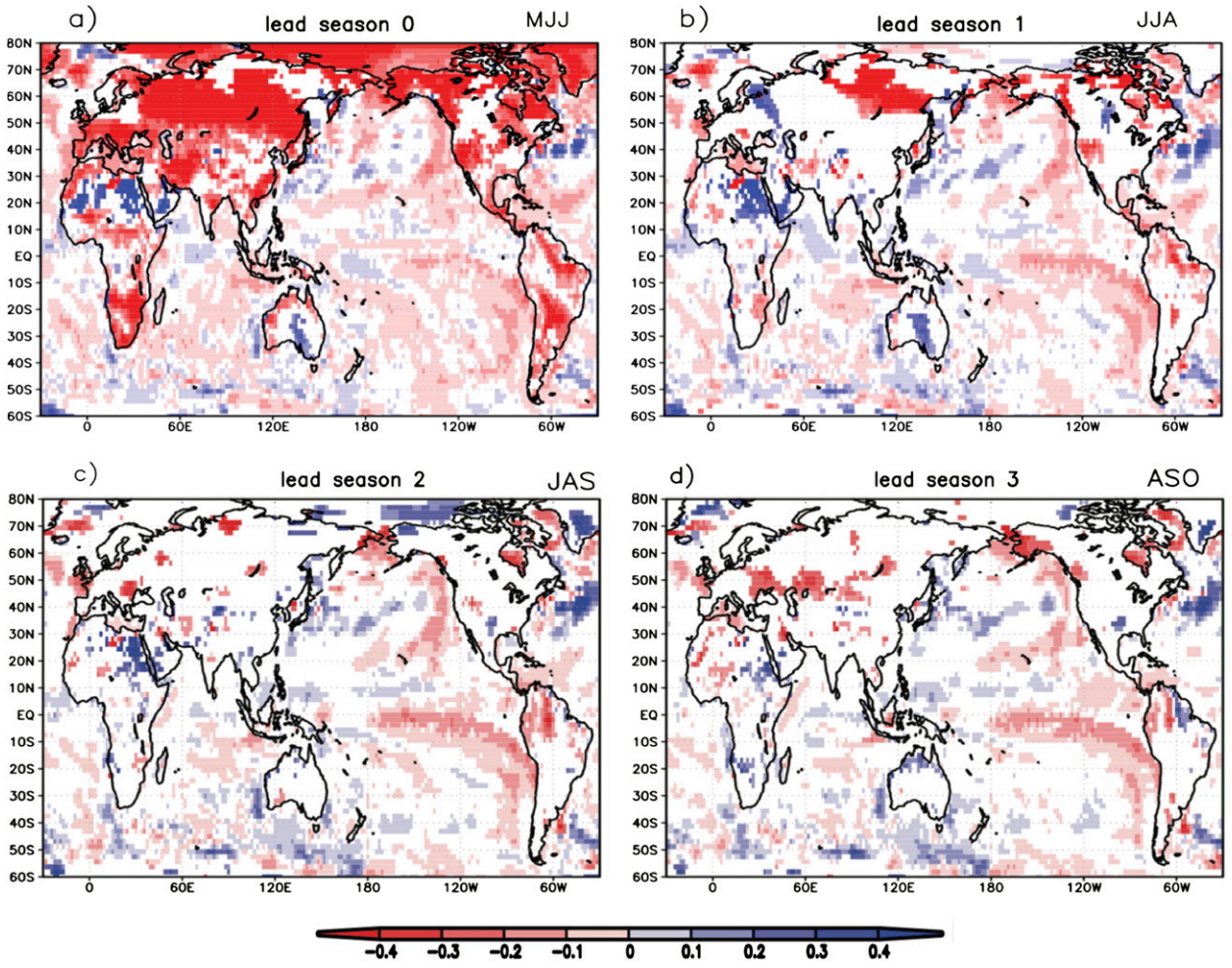

FIG. 6. RMSE (°C) difference between SPS2 and SPS1 for the start date of May, lead seasons 0–3. Shaded areas indicate differences significant at the 95% confidence level.

November, but some differences are also found for the other start dates (Table 2). Both the systems demonstrate very high skill in forecasting Niño-3.4 SST anomalies up to the end of the winter, and the relatively small spread of the ensemble members (extrapolated by the uncertainty bars in Fig. 10) confirms the high predictability of this region. Both SPS models tend to overestimate the amplitude of the most vigorous ENSO events, such as the 1997 El Niño and the 1999 La Niña, with SPS2 being generally closer to the observed anomalies.

4. Disentangling the relative contribution of atmosphere and land surface on the quality of the forecast

a. Global surface temperature

In addition to the analysis on the effect of atmosphere and land initialization on seasonal predictability, it is fundamental to understand the individual role of these two components. In an effort to discriminate between variations of the forecast due to the atmospheric or the land surface initial state, we designed an additional set of retrospective forecast. In this new configuration, the dynamical model is started with the same initial state as SPS2 for the ocean and the atmosphere, while land surface, similarly to SPS1, is initialized through an AMIP simulation. We label this new experiment SPS1.5. As for SPS1 and SPS2, here we only show results for the May and November start dates.

In Figs. 11 and 12 the impact of land surface initialization is highlighted, by displaying surface temperature ACC difference maps between SPS2 and SPS1.5. Red zones identify areas that benefit from the land surface initial state imparted by ERAI; blue areas have higher forecast skill in the noninitialized system. Results are strongly dependent on the start date; however, Figs. 11e and 12e show that, globally, the significant area of

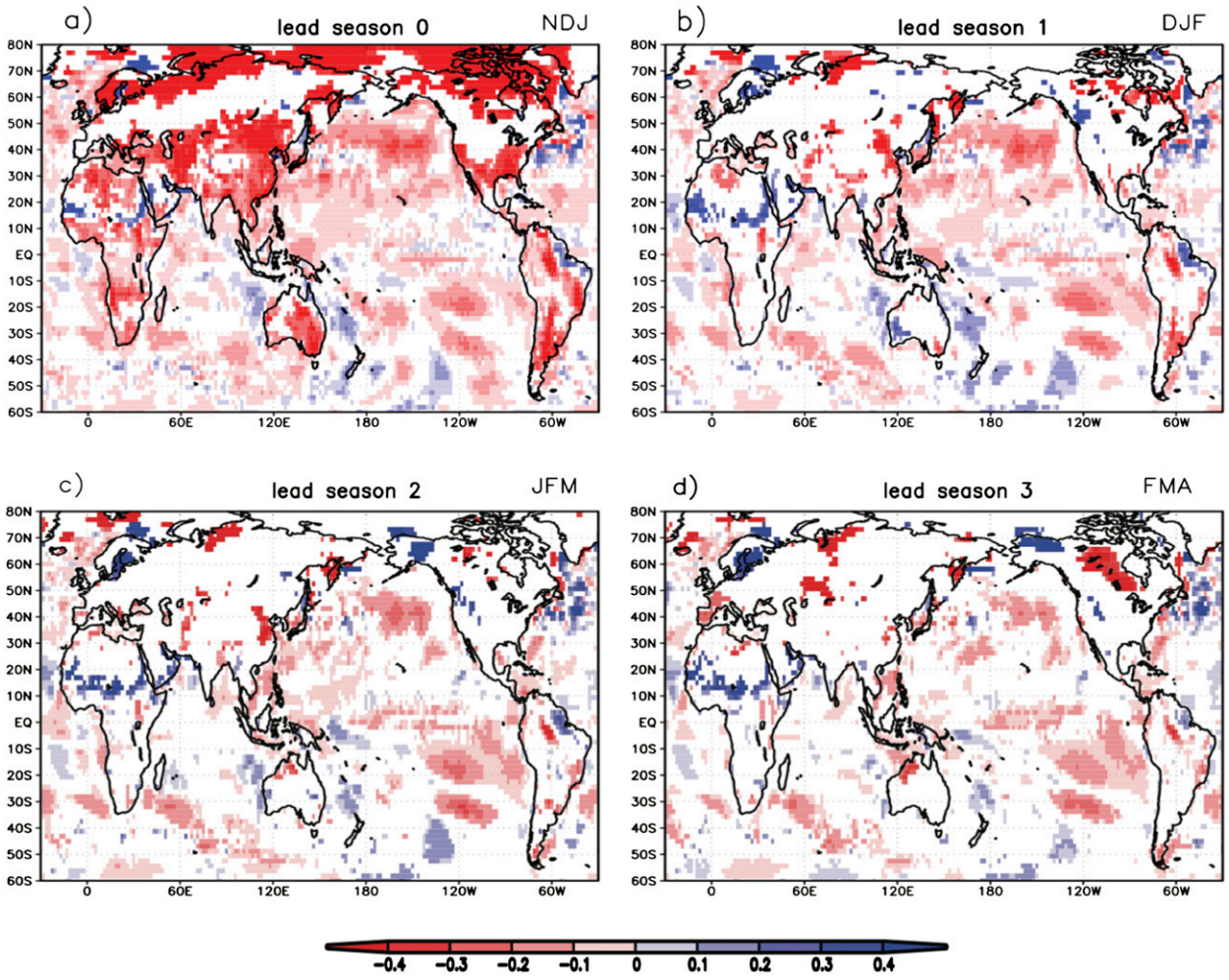

FIG. 7. As in Fig. 6, but for the start date of November.

improved skill always prevails over the area of skill reduction in both the forecasts. As expected, oceans are only impacted to a moderate extent, while continents are subject to major changes due to the land surface initialization, implying that the nonlocal effect of land surface is fairly small.

It is interesting to note that forecast skill and accuracy differences remain fairly consistent over time, with little displacement within successive lead seasons. This outcome suggests that memory conveyed by land surface characteristics may influence the climate system for several months, as already discussed in many recent works (see, e.g., Guo et al. 2011; Orth and Seneviratne 2012). This hypothesis can be confirmed comparing these differences to those between SPS2 and SPS1. Aside from the first lead month, which strongly influences lead season 0, most of the mainland patterns in Figs. 4b–d (Figs. 5b–d) can be found in Figs. 11b–d (Figs. 12b–d), indicating that large part of predictability is strictly determined by land surface initial condition. Likewise, RMSE differences seen in Figs. 6 and 7 are, beyond lead season 0, similar to those between SPS2 and SPS1.5 (not shown).

In November, surface temperatures of semiarid regions in central Asia and Africa benefit of the initialized surface features for most of the prediction time, as well as in eastern Canada (Fig. 12c). The improvement found over eastern Canada and northeastern Asia in the November forecast (Figs. 12b–d) may be a consequence of the initialization of snow depth, which was found to be a predictor for winter season at high latitudes (e.g., Cohen and Jones 2011). The Euro-Mediterranean region shows improvements especially in the May (Figs. 11c,d) and August (not shown) start date, most likely due to the strong land–atmosphere coupling which characterizes the hot season (Fischer et al. 2007), allowing for long-lasting forecast enhancements.

In this regard, exclusively for the May start date, our results are only partially consistent with recent studies in

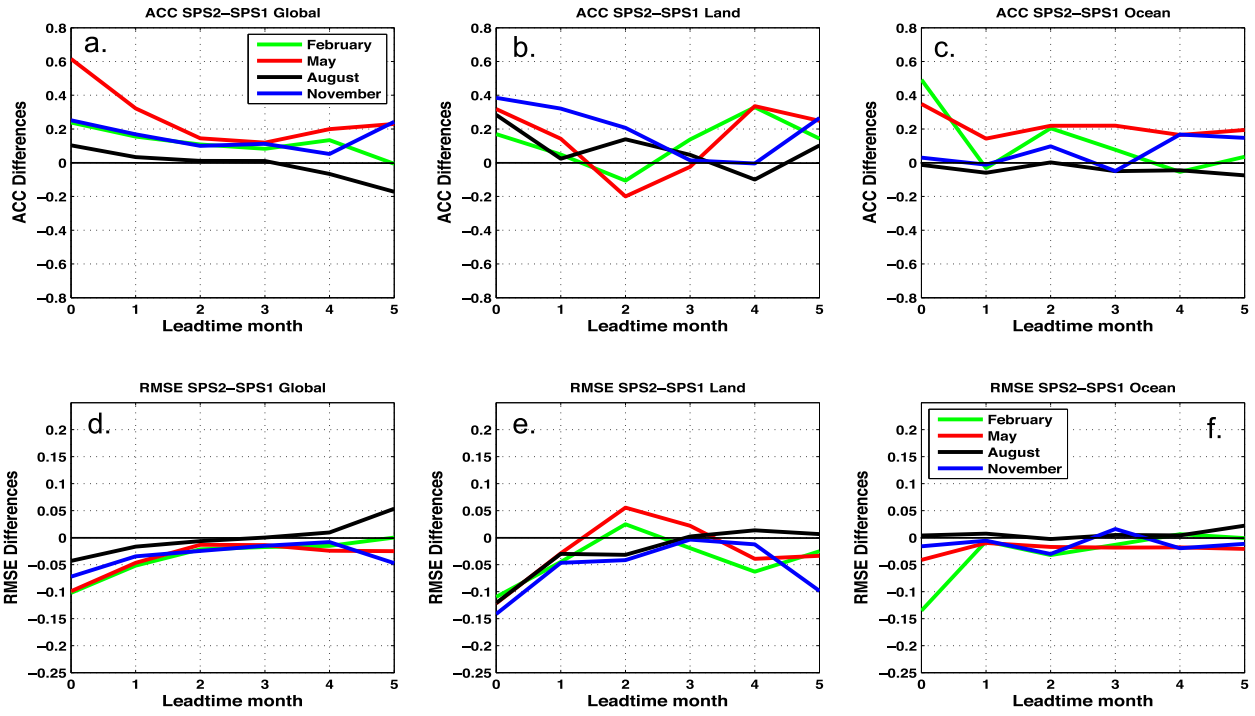

FIG. 8. (a)–(c) ACC and (d)–(f) RMSE (°C) of surface temperature, for the four start dates. Area averages over (left) global domain, (center) continental regions, and (right) oceans.

the frame of the second phase of the Global Land–Atmosphere Coupling Experiment (GLACE-2). In Europe, the influence of land–atmosphere initialization on temperature forecast is noticeable at lead season 0 and partly at lead season 1 (Figs. 4a,b), but again the atmosphere contribution, and not the land surface, is the strongest impacting component. The involvement of land surface initialization comes out at lead season 2 and 3 (Figs. 11c,d). Koster et al. (2010) found that, over the United States, realistic initialization of land surface has a significant impact on temperature forecast up to 45 days, and even longer in the western region. Our study as well suggests that, out of the entire North American region, only the U.S. West Coast and the mountain region of the United States preserves part of the significant skill gained through realistic initialization. Again though, the atmosphere, rather than land surface, seems to be the main driver for skill (cf. Figs. 4b and 11b). Similarly to Europe, the effect of land surface shows up at the end of the summer (Figs. 11c,d).

On the other hand, in Manchuria surface temperature is more accurately predicted by SPS1.5 in the November forecast (Figs. 12c,d). Likewise, SPS2 is significantly less skillful in the arid region of eastern Sahara, compared to SPS1.5. In the Southern Hemisphere, particularly in Australia, the response to the different land initial state is conflicting in the two start dates.

b. The evolution of soil moisture

Figure 13 shows the summer (JJA) and winter [December–February (DJF)] climatologies of soil moisture for the two forecast experiments and ERAI. More specifically, we display a soil moisture index, that is, a measure of wetness to which soil moisture is scaled, in order to account for the different parameterizations of the two models and make the two models comparable. The SILVA land model, responsible for the SPS1.5 and the SPS2 soil moisture output, and HTESSEL (Balsamo et al. 2009) have different number and depth of soil layers (see section 2b): here we compare the total moisture for the entire soil column.

The impact of initialization is remarkable in a few regions. The unrealistically high soil moisture, which almost saturates the Sahara desert in SPS1.5, is for the most part reset by the effect of the ERAI initial conditions, so that forecasts for North Africa become trustworthy (Figs. 13c,d). Similarly, central Asia is extremely wet in the noninitialized experiment, and a more realistic state of soil moisture at the beginning of the forecast dries out the terrain in a vast region ranging from the Caspian Sea to China. This substantial impact on soil moisture suggests a strong drift of the soil moisture toward the wetter model climatology. The two abovementioned regions show opposite responses in

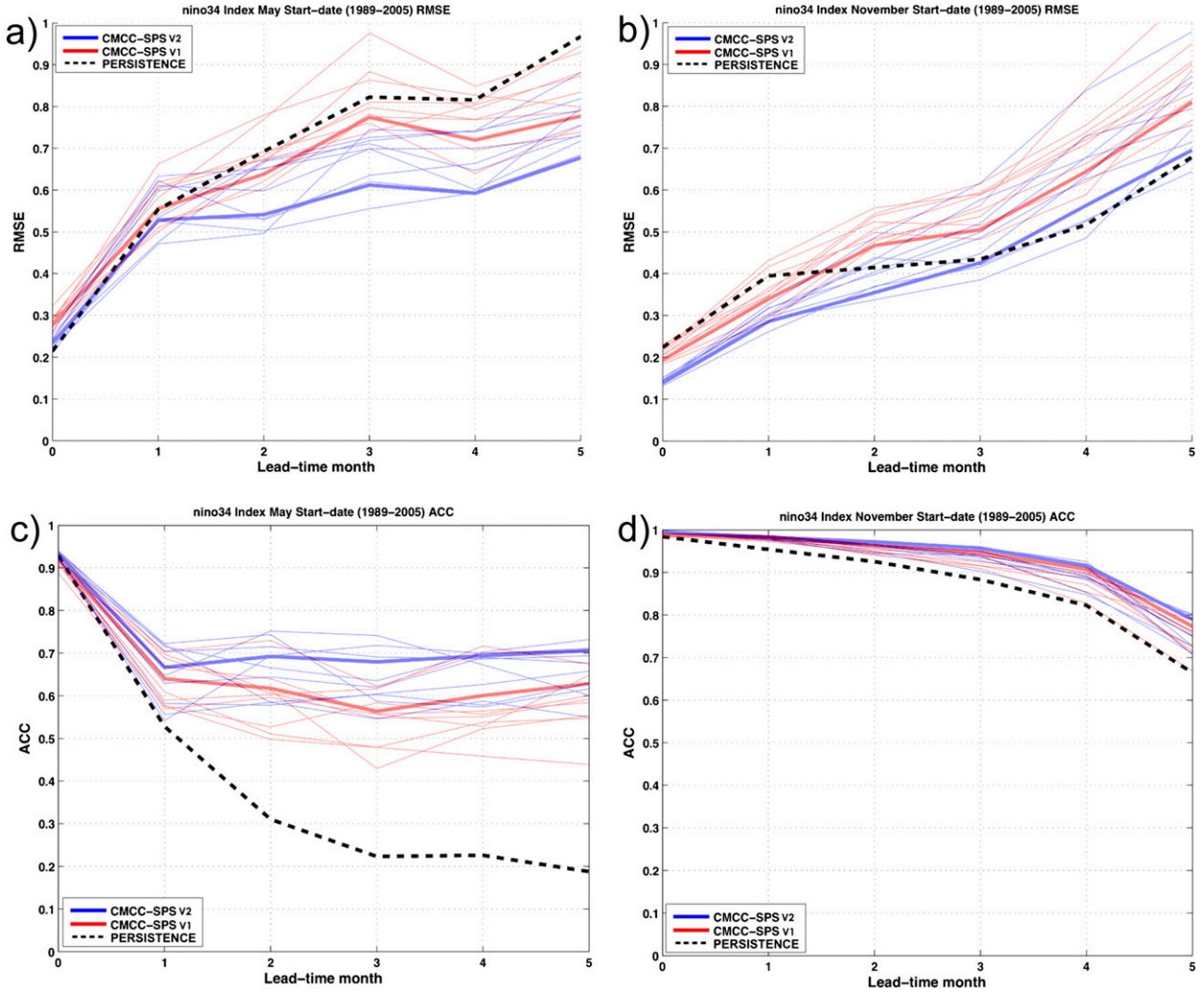

FIG. 9. RMSE (°C) of the Niño-3.4 index for SPS2 (blue lines) and SPS1 (red lines), for (a) May and (b) November start dates. Thick curves represent the ensemble mean of the nine members (thin curves). Also shown is the ACC of the Niño-3.4 index for SPS2 (blue lines) and SPS1 (red lines) for (c) May and (d) November start dates. Black dashed line represents persistence.

terms of surface temperature ACC: whereas in central Asia the land surface initialization leads to an improved skill in the forecast of November (Fig. 12), the quality of the May prediction is deteriorated in northeastern Africa (Fig. 11).

Soil moisture anomalies for the two regions in the start dates of interest are shown in Fig. 14. For each area, we selected the driest (Figs. 14a,d) and the wettest (Figs. 14b,e) initial observed conditions (i.e., ERAI soil moisture), averaging initial states exceeding the threshold of one standard deviation. Then we calculated the monthly anomaly until the end of the forecast for ERAI and the two prediction systems. As expected, anomalies in SPS2 are initially very close to that in observations, and the covariance between the two series remains very high for the entire forecast. In SPS1.5, the initial deviation from the mean is generally farther from ERAI's, and the evolution of soil moisture does not follow the observed.

Although progression in time of the anomalies is similar for soil moisture in central Asia and northeastern Africa, the response on surface temperature is the

TABLE 2. Correlation coefficients between predicted and observed Niño-3.4 index in lead season 1. Two asterisks indicate that the difference with SPS2 is statistically significant at the 95% level (using a *t* test).

System start date	SPS2	SPS1.5 (see section 4)	SPS1
February	0.92	0.92	0.90
May	0.70	0.69	0.62**
August	0.94	0.95	0.92
November	0.98	0.97	0.97

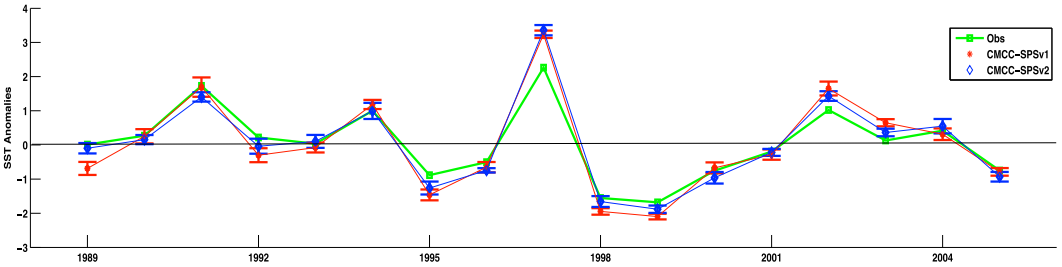

FIG. 10. Niño-3.4 SST anomalies as forecast in SPS1, SPS2, and observations. Lead season 1 of the November start date is displayed.

opposite. This might be due to the rapid drift of soil moisture to the model climatology in the African region (Fig. 14c), which creates an initialization shock that is likely to affect prediction of related variables such as surface temperatures (Dirmeyer et al. 2004). The drift exists in the Asia domain as well, but is considerably slower (Fig. 14f). Also, northeastern Africa is a severely water-limited area, where coupling between land surface and atmosphere is inhibited by the absence of the mediating role of evapotranspiration (Seneviratne et al. 2010). Therefore, surface temperature predictability in this region is plausibly independent from land initial conditions.

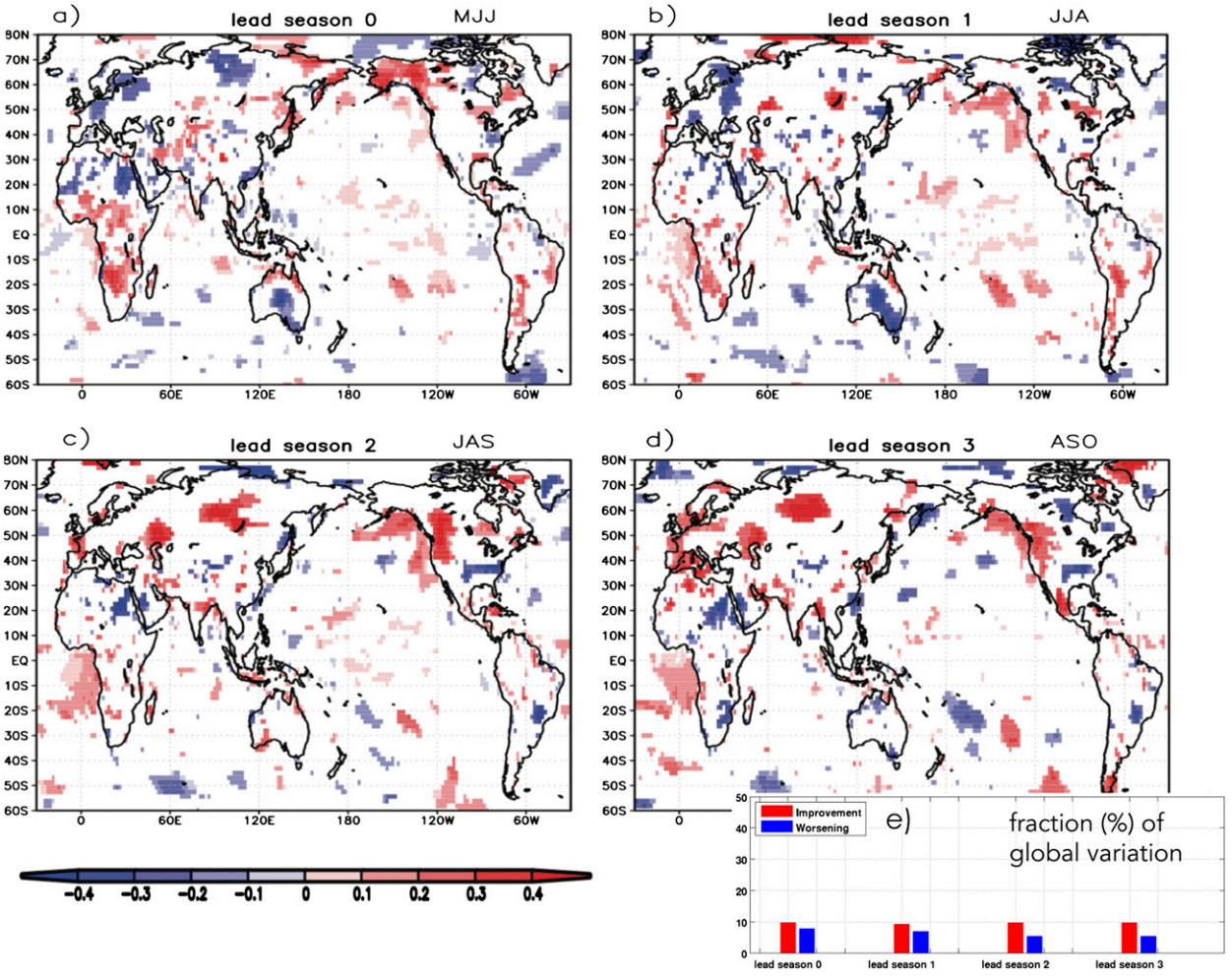

FIG. 11. (a)–(d) As in Fig. 4, but for the difference SPS2 − SPS1.5. (e) Percentage of significant variation in model skill after initialization of land surface.

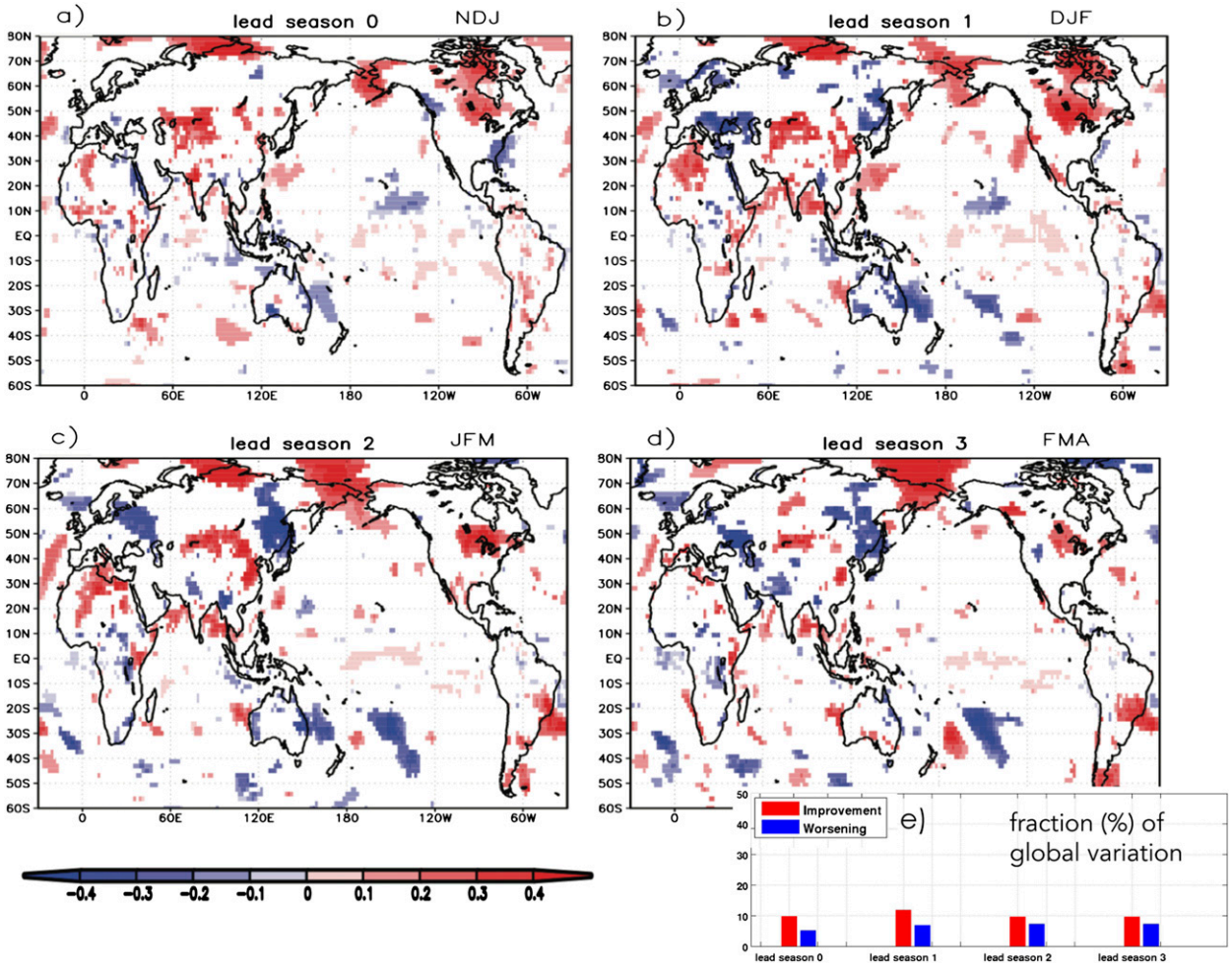

FIG. 12. (a)–(d) As in Fig. 5, but for the difference SPS2 − SPS1.5. (e) Percentage of significant variation in model skill after initialization of land surface.

c. *Regional effect of initialization*

Figures 15 and 16 summarize the impact of the different initialization strategies on forecast skill, examining 12 key regions covering a wide spectrum of climatic areas. Comparing SPS1 versus SPS1.5, it is possible to single out the contribution of the atmosphere initialization to ACC, since ocean (initialized through ocean reanalysis) and land (resulting from an AMIP-type experiment) initial states are identical in SPS1 and SPS1.5. Analogously, the difference between SPS1.5 and SPS2 identifies the role of land surface, as atmosphere and ocean models are identically initialized in the systems.

In the oceans, the quality of the forecast increases with the atmosphere initialization, while the initialization of land surface does not lead to further improvements. Over continental regions, the skill improvement may often be attributed to a realistic initial state of the atmosphere at lead season 0, when differences between SPS1.5 and SPS2 are generally smaller than those between SPS1.5 and SPS1 (Fig. 15, e.g., southern Europe, central Asia, and North Africa; Fig. 16, e.g., Australia and Amazonia). Areas covered by snow at the time of initialization (Fig. 16, e.g., Siberia, Canada, and central Asia) benefit from the land initialization from the beginning of the forecast. As time progresses, the information given by the initial land surface state becomes more important also for the remaining continental areas (Fig. 15, e.g., southern Europe and central Asia; Fig. 16, North Africa and northern India).

The nonlocal effect of land surface initial conditions can be evaluated by focusing on the ocean domains. Here, the skill of SST predictions is only minimally influenced by the initialization of land surface. Instead, the influence of the atmosphere is evident in regions of active air–sea coupling, such as the tropical South Pacific (see also section 3b). In the northern Pacific, the positive response to the atmosphere-only initialization in the

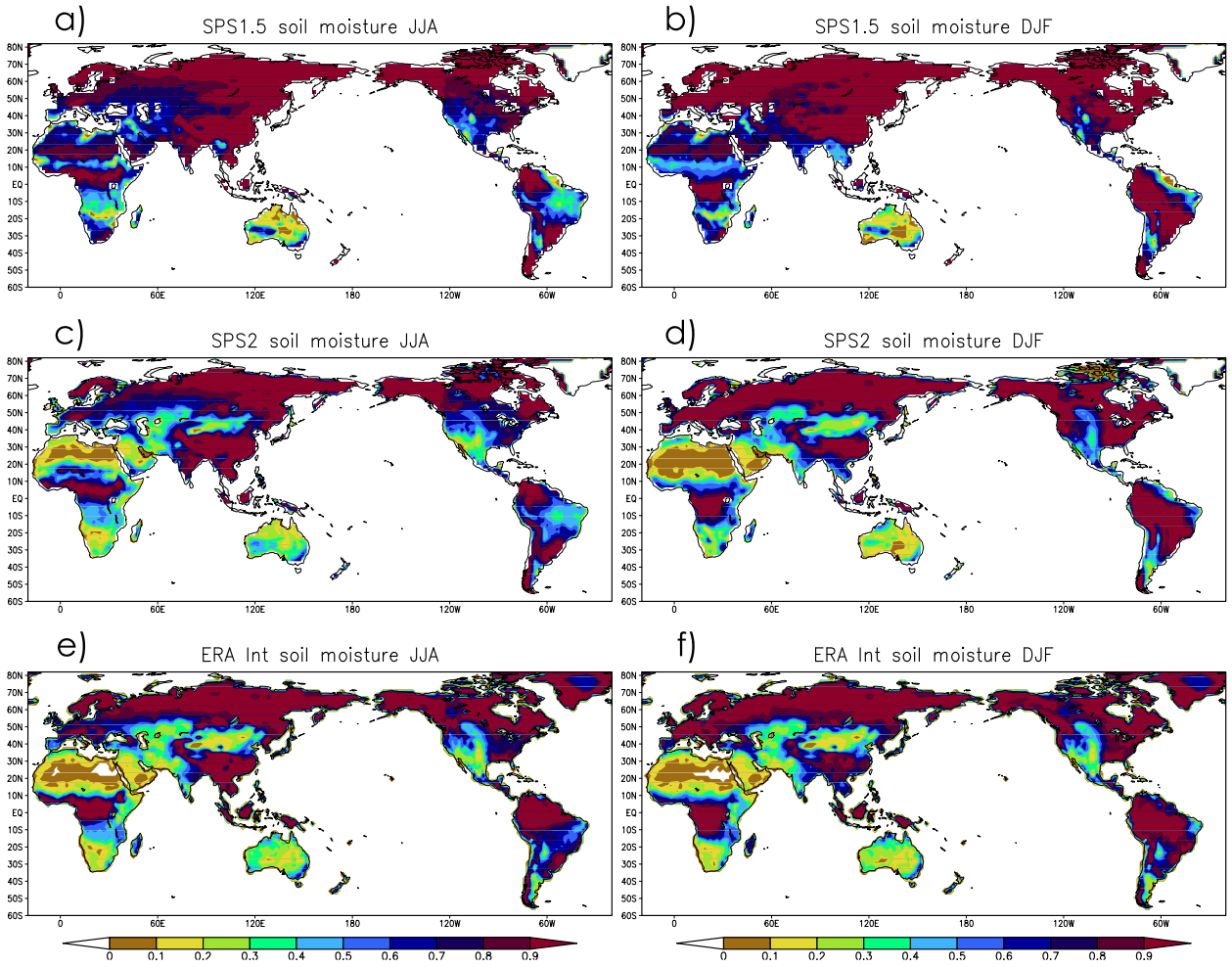

FIG. 13. (left) Summer (JJA) and (right) winter (DJF) soil moisture mean (shading) and standard deviation (contours), for (a),(b) SPS1.5, (c),(d) SPS2, and (e),(f) ERAI.

November start date (Fig. 16; see also Fig. 5) can be also attributed to the strong air–sea coupling taking place in this region. Frankignoul and Sennéchael (2007) suggest that SST anomalies force a Pacific–North American (PNA) pattern response in the autumn. The atmospheric reaction could in turn contribute to a change in the SST pattern, so that SST anomalies resemble that associated with the PNA.

The role of snow cover as a predictor of winter temperature (see Yang et al. 2001; Allen and Zender 2011) is examined by looking at the skill for the November forecast (Fig. 16). The increase in skill related to land surface initialization over eastern Canada and northern Siberia is most likely due to improved information on snow depth and cover, with positive repercussions on albedo and related feedbacks acting on surface temperatures. The influence on surface temperature lasts until the beginning of the following spring, that is, several months after initialization. At the beginning of February (not shown) and May (Fig. 15), these two regions are covered in snow in both SPS1.5 and SPS2, and differences in forecast skill are much reduced.

In midlatitudes, a major contributor to forecast skill has long been considered to be the soil moisture initial state (Fennessy and Shukla 1999; Dirmeyer 2003; Koster et al. 2004). The forecast in central Asia is affected by both land and atmosphere initialization: although the skill is low in this region, the quality of seasonal prediction gradually improves with the degree of realism in the initialization. A similar progressive improvement under SPS1, SPS1.5, and SPS2 initializations is found in southern Europe, in May (Fig. 15), when an accurate knowledge of the land surface initial state appears decisive. This information may be crucial as a predictor for summer heat waves in these areas. Besides, an increase in skill with time occurs in the summer forecast here. As

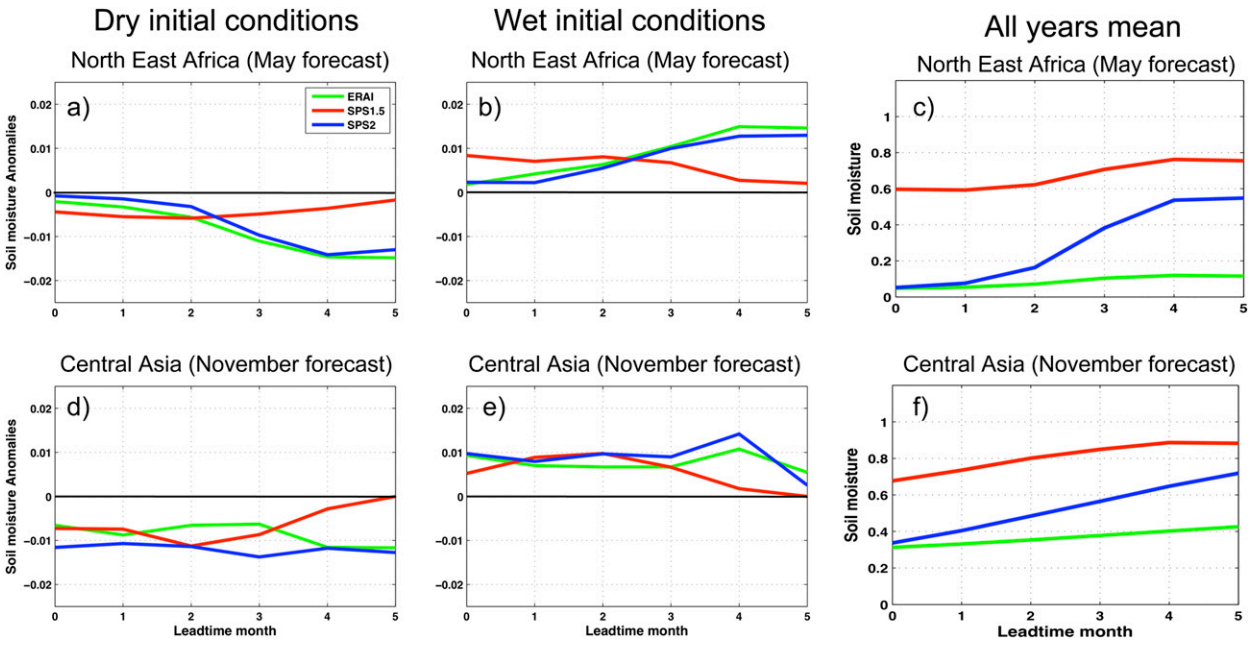

FIG. 14. Composite of soil moisture anomalies in the (a)–(c) May forecast for northeast Africa and (d)–(f) November forecast for central Asia, in the event of (left) dry and (center) wet initial conditions as measured in ERAI. (right) Full values of the 6-month forecast of soil moisture for the two start dates in the aforesaid regions.

recently discussed in a study of Guo et al. (2012), during late spring and summer there is a rebound of predictability of air temperature, because of information stored in the land surface that emerges when the coupling with atmosphere is stronger. This predictability rebound was found for North America, but it is reasonable to assume that a similar behavior affects other temperate regions. In Australia, the state of soil moisture impacts the forecast in both seasons: initial conditions imparted by reanalyses lead to a decline of the prediction skill.

5. Conclusions

We examined the influence of land–atmosphere initialization in a hierarchy of seasonal forecast experiments. Furthermore, we have made a first attempt to discriminate between the role played by atmosphere and land surface separately on the predictive skill of the forecast. To achieve these objectives, we compared three different versions of the CMCC Seasonal Prediction System, each differing for the initialization strategy.

In SPS2, the fully initialized version, forecast skill and accuracy are improved compared with the ocean-only initialized SPS1 system. We show that progresses in the quality of the forecast over the oceans can be largely attributed to the upgraded atmospheric initial condition. On the other hand, seasonal prediction skill on continental regions is primarily driven by land surface initialization.

The realistic initialization of air temperature and winds allows an improved equilibrium state between the ocean and overlying atmosphere, which possibly mitigates the coupling shock that often appears with the full-value initialization strategy, and ultimately strengthens the overall predictability. In a few specific regions, the coupling between the two components prolongs this positive effect throughout the whole forecast period. In the Niño-3.4 region, the SPS models have high predictability with large skill in all of the start dates. However, the summer (JJA) forecast skill is lower than the other seasons, possibly due to the so-called spring barrier effect, which is known to affect seasonal predictability in the equatorial Pacific. Nonetheless, the skill improvement provided by SPS2 to the summer forecast is statistically significant. Furthermore, the influence of the atmosphere initialization is highly significant in the northern Pacific and eastern tropical Atlantic for the November start date.

Over continental regions, the effect of atmospheric initial conditions is observable only in the early phase of the forecast, while most of the later changes in the forecast skill and accuracy can be ascribed to land surface initialization. In large parts of Canada, as well as northeastern Siberia, initialization of snow cover and depth largely determines the quality of the forecast started in late autumn, at the beginning of snow season.

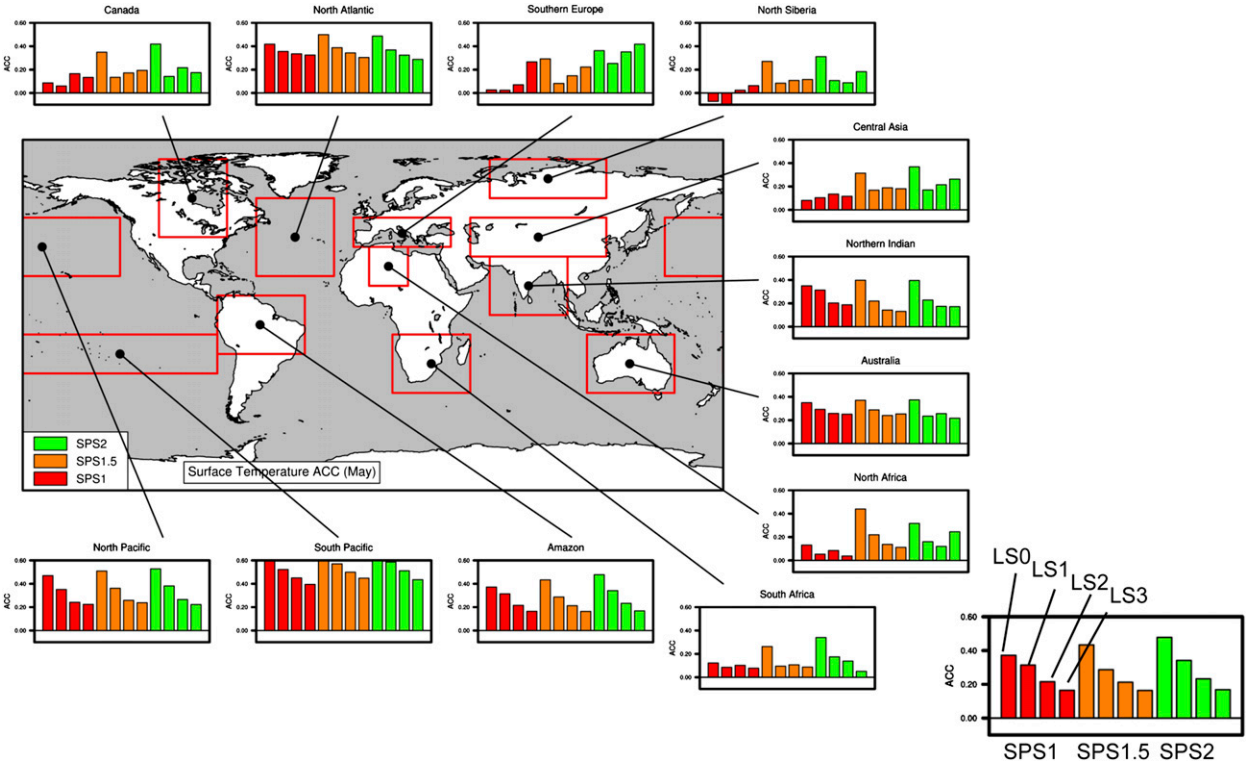

FIG. 15. ACC averaged in different regions for the May start date. (bottom right) The colors refer to the three versions of the CMCC-SPS; the bars refer to lead seasons 0–3.

In central Asia and southern Europe, the contribution of land surface is most likely attributable to soil moisture initialization, which is found to be a critical predictor in midlatitudes. In these regions, the quality of the forecast systematically improves as a consequence of upgraded initialization, with predictive skill progressing from zero to statistically significant positive values.

However, even though the influence of land state is unquestionable, forecast skill and accuracy are sometimes deteriorated by the surface initialization through ERAI. In fact, the use of full-value initialization for the land model could generate inconsistencies that degrade the quality of the forecast, with respect to that obtained with the AMIP-based initial condition. It is now common practice to use the Land Data Assimilation System approach (LDAS; see, e.g., Rodell et al. 2004), which does not assimilate observations to update the land state but rather lets the surface models evolve in response to the analysis of near-surface meteorological forcing (Yang et al. 2011). In fact, each land surface scheme has its own climatology for soil moisture and snow cover, which may differ substantially from another (Guo et al. 2006), and generates quite a contrasting response in the simulation of related quantities, such as river discharge (Materia et al. 2010). Soil moisture, above all, is a strongly model-specific quantity, closely related to the runoff formulation and the empirical parameters utilized in the model itself (Koster et al. 2009).

Moreover, the relatively small size of the forecast ensemble and the shortness of the hindcast period negatively impact on the signal-to-noise ratio. Therefore this analysis has to be considered with some caution: we cannot exclude that some regional features shown in Figs. 11 and 12 would be nonsignificant after considering either a larger ensemble size or a longer hindcast period.

These results may also suggest that ERAI land surface initial condition is not necessarily closer to reality than the initial state estimate provided by the land surface component of the coupled model (i.e., SILVA; see Fig. 1). In fact, variables such as soil moisture and snow cover are, in both cases, resulting from the response of a land surface scheme forced by model-generated precipitation, which may be inaccurate. Albergel et al. (2012) evaluated ERAI soil moisture versus 117 in situ stations across the world and concluded that, on average, the correlation between the two time series is $r = 0.63$. However, results are conditional on the biome and the climate, with a large spatial variability across different regions. More reliable estimates of soil moisture may be derived by rain gauge stations. In the GLACE-2

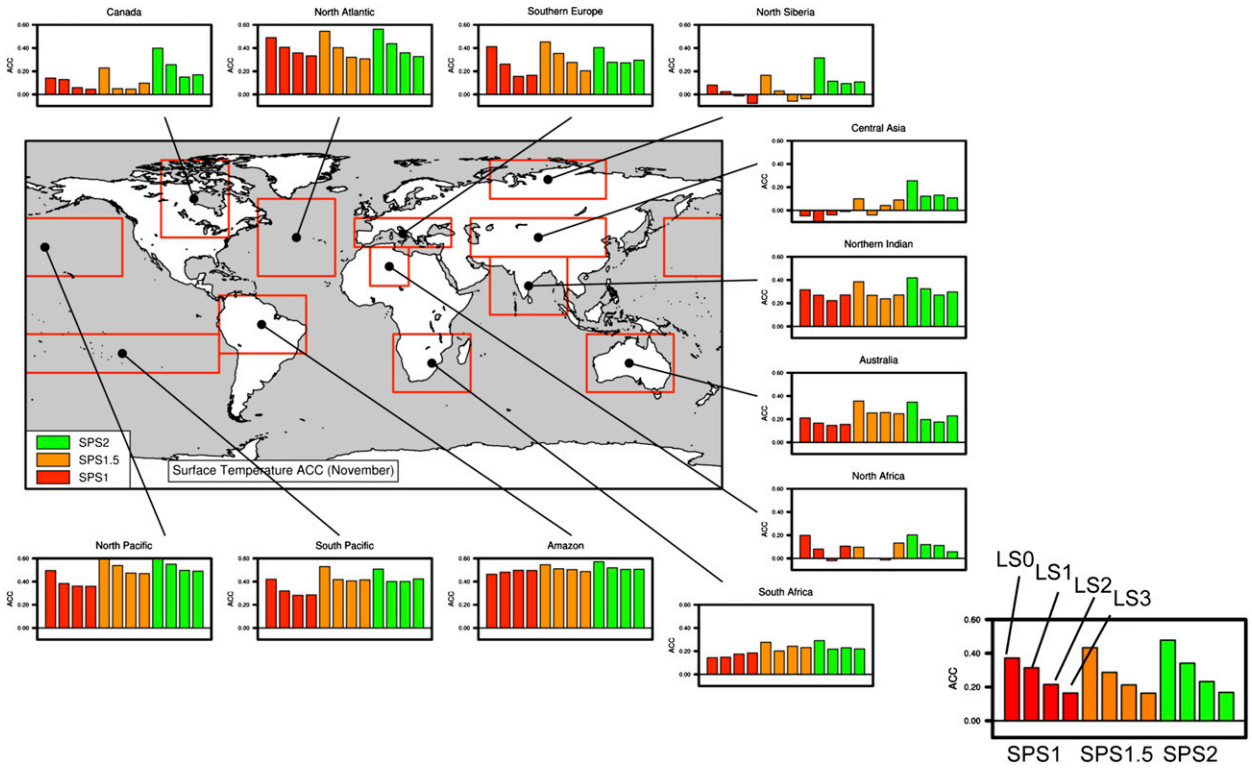

FIG. 16. As in Fig. 15, but for the November start date.

study, Koster et al. (2011) stated that significant impacts of soil moisture on air temperature are found in many regions, but the skill is limited to areas for which observational network of precipitation (used as a proxy for soil moisture) "provides adequate coverage and thus trustworthy initialization." Likewise, one may argue that even ERAI surface temperature may be biased by the lack of observations, especially in areas of the world (most of Africa and interior Asia) where data coverage is still scarce.

The full-value approach for the initialization of land state applied in this study may create some inconsistencies, which might negatively affect the results. Possibly, an anomaly initialization strategy, building the initial state with observed (here, ERAI) anomalies added to the model's own climatology, so as to avoid the spurious model adjustment following the initialization, would allow, at least in some cases, an improvement of surface temperature prediction. On the other hand, using this technique for land surface only, while keeping the full-state initialization for the atmosphere and the ocean, may generate some additional inconsistencies in the transient evolution of the system. We then prefer to maintain the standard full-value initialization for all three components, which has the advantage of more accurate information about land–air fluxes and the inclusion of the associated atmosphere variability (Balmaseda and Anderson 2009). However, our work represents a first step in this direction, and a similar experiment should be designed after a long run of the land surface scheme in an offline mode, driven by observations, in order to have a consistent soil wetness dataset for initialization.

In conclusion, the latest version of the CMCC-SPS has achieved a substantial improvement in the forecast skill and accuracy. Part of the enhanced predictive potential is due to the coupling mechanisms between the atmosphere and ocean, while improvements on continental areas appear to result from a realistic land surface initial state. To date, reanalyses are the best product available to set atmospheric initial conditions. For land surface, using more accurate datasets of soil moisture, snow, and vegetation will provide a significant step forward in the realization of valuable seasonal predictions.

Acknowledgments. This research was supported by the international project ClimAfrica, funded by European Commission under the 7th Framework Programme (FP7). The authors also acknowledge the support of the Italian Ministry of Education, University and Research and Ministry for Environment, Land and Sea through the Project GEMINA. Andrea Alessandri acknowledges the support of the European Commission's

FP7 Marie Curie projects CLIMITS under Grant Agreement 302208. Stefano Materia thanks Miss Page St. Clair for her precious editing work.

REFERENCES

Albergel, C., P. de Rosnay, G. Balsamo, L. Isaksen, and J. Muñoz-Sabater, 2012: Soil moisture analyses at ECMWF: Evaluation using global ground-based in situ observations. *J. Hydrometeor.,* **13,** 1442–1460, doi:10.1175/JHM-D-11-0107.1.

Alessandri, A., 2006: Effects of land surface and vegetation processes on the climate simulated by an atmospheric general circulation model. Ph.D. thesis, Bologna University Alma Mater Studiorum, 114 pp.

——, and A. Navarra, 2008: On the coupling between vegetation and rainfall inter-annual anomalies: Possible contributions to seasonal rainfall predictability over land areas. *Geophys. Res. Lett.,* **35,** L02718, doi:10.1029/2007GL032415.

——, A. Borrelli, S. Masina, A. Cherchi, S. Gualdi, A. Navarra, P. Di Pietro, and A. F. Carril, 2010: The INGV–CMCC seasonal prediction system: Improved ocean initial conditions. *Mon. Wea. Rev.,* **138,** 2930–2952, doi:10.1175/2010MWR3178.1.

——, ——, A. Navarra, A. Arribas, M. Déqué, P. Rogel, and A. Weisheimer, 2011: Evaluation of probabilistic quality and value of the ENSEMBLES multimodel seasonal forecasts: Comparison with DEMETER. *Mon. Wea. Rev.,* **139,** 581–607, doi:10.1175/2010MWR3417.1.

——, P. G. Fogli, M. Vichi, and N. Zeng, 2012: Strengthening of the hydrological cycle in future scenarios: Atmospheric energy and water balance perspective. *Earth Syst. Dyn.,* **3,** 199–212, doi:10.5194/esd-3-199-2012.

Allen, R. J., and C. S. Zender, 2011: Forcing of the Arctic Oscillation by Eurasian snow cover. *J. Climate,* **24,** 6528–6539, doi:10.1175/2011JCLI4157.1.

Alves, O., M. A. Balmaseda, D. Anderson, and T. Stockdale, 2004: Sensitivity of dynamical seasonal forecasts to ocean initial conditions. *Quart. J. Roy. Meteor. Soc.,* **130,** 647–667, doi:10.1256/qj.03.25.

Balmaseda, M. A., and D. Anderson, 2009: Impact of initialization strategies and observations on seasonal forecast skill. *Geophys. Res. Lett.,* **36,** L01701, doi:10.1029/2008GL035561.

——, and Coauthors, 2009: Ocean initialization for seasonal forecasts. *Oceanography,* **22,** 154–159, doi:10.5670/oceanog.2009.73.

Balsamo, G., P. Viterbo, A. Beljaars, B. van den Hurk, M. Hirschi, A. K. Betts, and K. Scipal, 2009: A revised hydrology for the ECMWF model: Verification from field site to terrestrial water storage and impact in the Integrated Forecast System. *J. Hydrometeor.,* **10,** 623–643, doi:10.1175/2008JHM1068.1.

Bellucci, A., S. Masina, P. DiPietro, and A. Navarra, 2007: Using temperature–salinity relations in a global ocean implementation of a multivariate data assimilation scheme. *Mon. Wea. Rev.,* **135,** 3785–3807, doi:10.1175/2007MWR1821.1.

Berrisford, P., D. Dee, K. Fielding, M. Fuentes, P. Kallberg, S. Kobayashi, and S. Uppala, 2009: The ERA Interim archive. Tech. Rep. ERA Rep. Series 1, ECMWF, 16 pp. [Available online at http://old.ecmwf.int/publications/library/do/references/list/782009.]

Blender, R., and K. Fraedrich, 2003: Long time memory in global warming simulations. *Geophys. Res. Lett.,* **30,** 1769, doi:10.1029/2003GL017666.

Borrelli, A., S. Materia, A. Bellucci, A. Alessandri, and S. Gualdi, 2012: Seasonal Prediction System at CMCC. Research Paper 147, Centro Euro-Mediterraneo sui Cambiamenti Climatici, 17 pp. [Available at http://www.cmcc.it/publications-meetings/publications/research-papers/rp0147-seasonal-prediction-system-at-cmcc.]

Chen, D., M. A. Cane, A. Kaplan, S. E. Zebiak, and D. Huang, 2004: Predictability of El Niño over the past 148 years. *Nature,* **428,** 733–736, doi:10.1038/nature02439.

Cohen, J., and J. Jones, 2011: A new index for more accurate winter predictions. *Geophys. Res. Lett.,* **38,** L21701, doi:10.1029/2011GL049626.

Dirmeyer, P. A., 2003: The role of the land surface background state in climate predictability. *J. Hydrometeor.,* **4,** 599–610, doi:10.1175/1525-7541(2003)004<0599:TROTLS>2.0.CO;2.

——, Z. Guo, and X. Gao, 2004: Comparison, validation, and transferability of eight multiyear global soil wetness products. *J. Hydrometeor.,* **5,** 1011–1033, doi:10.1175/JHM-388.1.

Douville, H., 2003: Assessing the influence of soil moisture on seasonal climate variability with AGCMs. *J. Hydrometeor.,* **4,** 1044–1066, doi:10.1175/1525-7541(2003)004<1044:ATIOSM>2.0.CO;2.

Fennessy, M. J., and J. Shukla, 1999: Impact of initial soil wetness on seasonal atmospheric prediction. *J. Climate,* **12,** 3167–3180, doi:10.1175/1520-0442(1999)012<3167:IOISWO>2.0.CO;2.

Fischer, E. M., S. Seneviratne, D. Lüthi, and C. Schär, 2007: Contribution of land–atmosphere coupling to recent European summer heatwaves. *Geophys. Res. Lett.,* **34,** L06707, doi:10.1029/2006GL029068.

Fogli, P. G., and Coauthors, 2009: INGV-CMCC Carbon (ICC): A Carbon Cycle Earth System Model. CMCC Research Paper 61, 31 pp. [Available at http://www.cmcc.it/publications-meetings/publications/research-papers/rp0061-ingv-cmcc-carbon-icc-a-carbon-cycle-earth-system-model.]

Frankignoul, C., and N. Sennéchael, 2007: Observed influence of North Pacific SST anomalies on the atmospheric circulation. *J. Climate,* **20,** 592–606, doi:10.1175/JCLI4021.1.

Guo, Z., P. A. Dirmeyer, Z.-Z. Hu, X. Gao, and M. Zhao, 2006: Evaluation of the Second Global Soil Wetness Project soil moisture simulations: 2. Sensitivity to external meteorological forcing. *J. Geophys. Res.,* **111,** D22S03, doi:10.1029/2006JD007845.

——, ——, and T. DelSole, 2011: Land surface impacts on subseasonal and seasonal predictability. *Geophys. Res. Lett.,* **38,** L24812, doi:10.1029/2011GL049945.

——, ——, ——, and R. D. Koster, 2012: Rebound in atmospheric predictability and the role of the land surface. *J. Climate,* **25,** 4744–4749, doi:10.1175/JCLI-D-11-00651.1.

Hoskins, B., and P. S. Schopf, 2008: Ocean–atmosphere basis for seasonal climate forecasting. *Seasonal Climate: Forecasting and Managing Risk,* A. Troccoli et al., Eds., Springer, 67–89.

Hudson, D., O. Alves, H. H. Hendon, and G. Wang, 2011: The impact of atmospheric initialisation on seasonal prediction of tropical Pacific SST. *Climate Dyn.,* **36,** 1155–1171, doi:10.1007/s00382-010-0763-9.

Iwi, A. M., R. T. Sutton, and W. A. Norton, 2006: Influence of May Atlantic Ocean initial conditions on the subsequent North Atlantic winter climate. *Quart. J. Roy. Meteor. Soc.,* **132,** 2977–2999, doi:10.1256/qj.05.62.

Jeong, J.-H., C.-H. Ho, D. Chen, and T.-W. Park, 2008: Land surface initialization using an offline CLM3 simulation with the GSWP-2 forcing dataset and its impact on CAM3 simulations of the boreal summer climate. *J. Hydrometeor.,* **9,** 1231–1248, doi:10.1175/2008JHM941.1.

Kim, H. M., P. J. Webster, and J. A. Curry, 2012: Seasonal prediction skill of ECMWF System 4 and NCEP CFSv2 retrospective

forecast for the Northern Hemisphere winter. *Climate Dyn.,* **39,** 2957–2973, doi:10.1007/s00382-012-1364-6.

Koster, R. D., and M. J. Suarez, 2003: Impact of land surface initialization on seasonal precipitation and temperature prediction. *J. Hydrometeor.,* **4,** 408–423, doi:10.1175/1525-7541(2003)4<408:IOLSIO>2.0.CO;2.

——, and ——, 2004: Suggestions in the observational record of land–atmosphere feedback operating at seasonal time scales. *J. Hydrometeor.,* **5,** 567–572, doi:10.1175/1525-7541(2004)005<0567:SITORO>2.0.CO;2.

——, and Coauthors, 2004: Regions of strong coupling between soil moisture and precipitation. *Science,* **305,** 1138–1140, doi:10.1126/science.1100217.

——, Z. Guo, R. Yang, P. A. Dirmeyer, K. Mitchell, and M. J. Puma, 2009: On the nature of soil moisture in land surface models. *J. Climate,* **22,** 4322–4335, doi:10.1175/2009JCLI2832.1.

——, and Coauthors, 2010: Contribution of land surface initialization to subseasonal forecast skill: First results from a multi-model experiment. *Geophys. Res. Lett.,* **37,** L02402, doi:10.1029/2009GL041677.

——, and Coauthors, 2011: Contribution of land surface initialization to subseasonal forecast skill: The Second Phase of the Global Land–Atmosphere Coupling Experiment: Soil moisture contributions to subseasonal forecast skill. *J. Hydrometeor.,* **12,** 805–822, doi:10.1175/2011JHM1365.1.

Kug, J. S., I. S. Kang, and D. H. Choi, 2008: Seasonal climate predictability with tier-one and tier-two prediction systems. *Climate Dyn.,* **31,** 403–416, doi:10.1007/s00382-007-0264-7.

Madec, G., and M. Imbard, 1996: A global ocean mesh to overcome the North Pole singularity. *Climate Dyn.,* **12,** 381–388, doi:10.1007/BF00211684.

——, P. Delecluse, I. Imbard, and C. Levy, 1998: OPA 8.1 ocean general circulation model reference manual. Note du Pôle de modélisation 11, IPSL, 91 pp.

Masina, S., P. Di Pietro, A. Storto, and A. Navarra, 2011: Global ocean re-analyses for climate applications. *Dyn. Atmos. Oceans,* **52,** 341–366, doi:10.1016/j.dynatmoce.2011.03.006.

Materia, S., P. A. Dirmeyer, Z. Guo, A. Alessandri, and A. Navarra, 2010: The sensitivity of simulated river discharge to land surface representation and meteorological forcings. *J. Hydrometeor.,* **11,** 334–351, doi:10.1175/2009JHM1162.1.

McPhaden, M. J., and Coauthors, 1998: The Tropical Ocean–Global Atmosphere observing system: A decade of progress. *J. Geophys. Res.,* **103,** 14 169–14 240, doi:10.1029/97JC02906.

Navarra, A., 2002: Ensembles, forecasts and predictability. *Ocean Forecasting: Conceptual Basis and Applications,* N. Pinardi and J. Woods, Eds., Springer-Verlag, 131–148.

Orth, R., and S. I. Seneviratne, 2012: Analysis of soil moisture memory from observations in Europe. *J. Geophys. Res.,* **117,** D15115, doi:10.1029/2011JD017366.

Palmer, T. N., F. J. Doblas-Reyes, A. Weisheimer, and M. J. Rodwell, 2008: Toward seamless prediction: Calibration of climate change projections using seasonal forecasts. *Bull. Amer. Meteor. Soc.,* **89,** 459–470, doi:10.1175/BAMS-89-4-459.

Paolino, D. A., J. L. Kinter, B. P. Kirtman, D. Min, and D. M. Straus, 2012: The impact of land surface and atmospheric initialization on seasonal forecasts with CCSM. *J. Climate,* **25,** 1007–1021, doi:10.1175/2011JCLI3934.1.

Rayner, N. A., P. Brohan, D. E. Parker, C. K. Folland, J. J. Kennedy, M. Vanicek, T. J. Ansell, and S. F. B. Tett, 2006: Improved analyses of changes and uncertainties in sea surface temperature measured in situ since the mid-nineteenth century: The HadSST2 dataset. *J. Climate,* **19,** 446–469, doi:10.1175/JCLI3637.1.

Rodell, M., and Coauthors, 2004: The Global Land Data Assimilation System. *Bull. Amer. Meteor. Soc.,* **85,** 381–394, doi:10.1175/BAMS-85-3-381.

Roeckner, E., and Coauthors, 2003: The atmospheric general circulation model ECHAM5. Part I: Model description. MPI Rep. 349, 127 pp.

——, and Coauthors, 2006: Sensitivity of simulated climate to horizontal and vertical resolution in the ECHAM5 atmosphere model. *J. Climate,* **19,** 3771–3791, doi:10.1175/JCLI3824.1.

Seneviratne, S. I., T. Corti, E. L. Davin, M. Hirschi, E. B. Jaeger, I. Lehner, B. Orlowsky, and A. J. Teuling, 2010: Investigating soil moisture–climate interactions in a changing climate: A review. *Earth-Sci. Rev.,* **99,** 125–161, doi:10.1016/j.earscirev.2010.02.004.

Shi, L., H. Hendon, O. Alves, M. Wheeler, D. Anderson, and G. Wang, 2011: On the importance of initializing the stochastic part of the atmosphere for forecasting the 1997/1998 El Niño. *Climate Dyn.,* **37,** 313–324, doi:10.1007/s00382-010-0933-9.

Shukla, J., and J. C. Kinter, 2006: Predictability of seasonal climate variations: A pedagogical review. *Predictability of Weather and Climate,* T. Palmer and R. Hagedorn, Eds., Cambridge University Press, 306–341.

Smith, D. M., A. Scaife, and P. Kirtman, 2012: What is the current state of scientific knowledge with regard to seasonal and decadal forecasting? *Environ. Res. Lett.,* **7,** 015602, doi:10.1088/1748-9326/7/1/015602.

Timmermann, R., H. Goosse, G. Madec, T. Fichefet, C. Ethe, and V. Dulière, 2005: On the representation of high latitude processes in the ORCA-LIM global coupled sea ice–ocean model. *Ocean Modell.,* **8,** 175–201, doi:10.1016/j.ocemod.2003.12.009.

Trenberth, K. E., 1998. Development and forecasts of the 1997/98 El Niño: CLIVAR scientific issues. *CLIVAR Exchanges,* No. 3, International CLIVAR Project Office, Southampton, United Kingdom, 4–14.

——, and J. Caron, 2000: The Southern Oscillation revisited: Sea level pressures, surface temperatures, and precipitation. *J. Climate,* **13,** 4358–4365, doi:10.1175/1520-0442(2000)013<4358:TSORSL>2.0.CO;2.

Troccoli, A., M. Harrison, D. L. T. Anderson, and S. J. Mason, 2008: *Seasonal Climate: Forecasting and Managing Risk.* NATO Science Series, Vol. 82, Springer Academic, 499 pp.

Valcke, S., L. Terray, and A. Piacentini, 2000: The OASIS coupled user guide version 2.4. CERFACS Tech. Rep. TR/CMGC/00/10. [Available online at www.cerfacs.fr/3-25801-Technical-Reports.php.]

Vialard, J., F. Vitart, M. A. Balmaseda, T. Stockdale, and D. L. T. Anderson, 2005: An ensemble generation method for seasonal forecasting with an ocean–atmosphere coupled model. *Mon. Wea. Rev.,* **133,** 441–453, doi:10.1175/MWR-2863.1.

Vidard, A., D. L. T. Anderson, and M. Balmaseda, 2007: Impact of ocean observation systems on ocean analysis and seasonal forecasts. *Mon. Wea. Rev.,* **135,** 409–429, doi:10.1175/MWR3310.1.

Yang, F., A. Kumar, W. Wang, H. H. Juang, and M. Kanamitsu, 2001: Snow–albedo feedback and seasonal climate variability over North America. *J. Climate,* **14,** 4245–4248, doi:10.1175/1520-0442(2001)014<4245:SAFASC>2.0.CO;2.

Yang, R., K. Mitchell, J. Meng, and M. Ek, 2011: Summer-season forecast experiments with the NCEP Climate Forecast System using different land models and different initial land states. *J. Climate,* **24,** 2319–2334, doi:10.1175/2010JCLI3797.1.